PRODUCTION OF PIONS AND ANOMALOUS PROJECTILE FRAGMENTS IN HEAVY ION COLLISIONS.

by

Birgitta Norén

Lund 1988

PRODUCTION OF PIONS AND

ANOMALOUS PROJECTILE FRAGMENTS

IN HEAVY ION COLLISIONS.

by

Birgitta Norén

COSMIC AND SUBATOMIC PHYSICS REPORT
LUIP 8804
LUNFD6/(NFFK-7087)1-101(1988)
ISSN 0348-9329

PRODUCTION OF PIONS AND ANOMALOUS PROJECTILE FRAGMENTS IN HEAVY ION COLLISIONS.

by

Birgitta Norén

AKADEMISK AVHANDLING SOM FÖR AVLÄGGANDE AV FILOSOFIE DOKTORSEXAMEN VID LUNDS UNIVERSITETS MATEMATISK-NATURVETENSKAPLIGA FAKULTET OFFENTLIGEN KOMMER ATT FÖRSVARAS I FÖRELÄSNINGSSAL B PÅ FYSISKA INSTITUTIONEN FREDAGEN DEN 3 JUNI 1988 KLOCKAN 14.15.

Organization LUND UNIVERSITY	Document name DOCTORAL DISSERTATION
	Date of issue May 1988
	CODEN: LUNFD6/(NFFK-7087)1-101(1988)
Author(s) Birgitta Norén	Sponsoring organization

Title and subtitle: PRODUCTION OF PIONS AND ANOMALOUS PROJECTILE FRAGMENTS IN HEAVY ION COLLISIONS.

Abstract: Results are presented from investigations of the mean free path (mfp) of multiply charged fragments, produced by 1.8 A GeV argon nuclei. The mfp's have been studied experimentally, and no dependence of the mfp on the distance from the preceeding collision is observed. In a Monte Carlo simulation, the mfp estimators are investigated for different statistics, with or without an enhanced reaction probability.

Intermediate energy heavy ion collisions have been studied using the carbon beam produced at the CERN SC-accelerator. Cross-sections for π^+ and π^- have been measured over a wide range of angles and targets. Also, coincidence measurements with projectile-like fragments have been performed. The π^-/π^+ ratio has been studied for C+Li, C+C, C+Pb, C+^{116}Sn and C+^{124}Sn. Inconsistencies in the target mass dependence of the pion yield disappear if a correction for reabsorption in the target nucleus is included. The projectile breakup is significantly stronger for pion producing collisions than for the average collision, thus indicating a much stronger abundance of central collisions.

Key words: Mean free path, Mean free path estimators, Heavy ion collisions, Intermediate energy, Pion production, Projectile breakup, Coincidence measurements, Isospin ratios.

Classification system and/or index terms (if any)

LUIP No 8804

Supplementary bibliographical information

Language: English

ISSN and key title: ISSN 0348-9329

ISBN: 91-7900-513-6

Recipient's notes

Number of pages: 101

Price

Security classification

Distribution by (name and address) Birgitta Norén, Department of Physics, University of Lund, Sölvegatan 14, S-223 62 LUND, Sweden.

I, the undersigned, being the copyright owner of the abstract of the above-mentioned dissertation, hereby grant to all reference sources permission to publish and disseminate the abstract of the above-mentioned dissertation.

Signature Birgitta Norén Date 3/5 1988

DOKUMENTDATABLAD enl SIS 61 41 21

I N T R O D U C T I O N

In this thesis, five papers are presented which are dealing with two topics in the field of heavy ion physics. The five publications are

1. Search for anomalous fragments in 1.8 A GeV ^{40}Ar reactions in nuclear emulsions.
   Phys. Rev. Lett. 54(1985)771.

2. Monte Carlo simulations of anomalon experiments.
   Nucl. Instr. and Methods B17(1986)265.

3. Subthreshold pion production in heavy-ion collisions at 85 A MeV.
   Phys. Rev. Lett. 48(1982)732.

4. Production of charged pions in intermediate energy heavy-ion collisions.
   Nucl. Phys. A423(1984)511.

5. Charged pion production and projectile breakup in 85 A MeV ^{12}C induced heavy ion reactions.
   Cosmic and Subatomic Physics Report LUIP 8802, 1988.
   Submitted to Nuclear Physics A.

The first two papers cover investigations of enhanced reaction probabilities for nuclear fragments, which are popularly called "anomalons". Papers 3-5 deal with the production of pions below the threshold of free nucleon-nucleon interactions in heavy ion collisions.

The chronological order of these papers are 3, 4, 1, 2 and 5, as I was first introduced into the field of heavy ion reaction physics with studies of pion production. Then, there arose a sudden and intense interest in the investigation of "anomalons", and since we by tradition master the nuclear emulsion technique, our involvement was almost self-evident. After this episode, the studies of pion

production were resumed and, in contrast to "anomalons", our commitment to this topic is still strong.

This thesis has been divided into five major sections, where the first and second one deal with studies of anomalous nuclear fragments. In the first, our emulsion experiment is presented, and a brief introduction to the conception of "anomalons" is given. In this section, I have also included a short description of some of the properties of nuclear emulsions. The computer based work in the Monte Carlo simulations on anomalon experiments is presented separately in section two. Details about the simulations are presented here, and the mean free path estimators are discussed.

Section three covers the pion experiments treated as a whole, where a short introduction into this field is also given. Methods for detecting and identifying charged pions are presented and at the end of this section, some results from these experiments are discussed. In the fourth section, a summary of the five publications are given, and in the last section the papers are presented in their published form.

Lund, May 1988

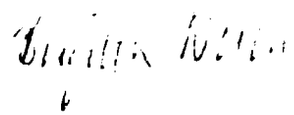

1. THE ANOMALON EPISODE

Before the seventies, when powerful heavy ion accelerators became available, high energy heavy ion physics consisted solely of studies of cosmic rays. Nuclear emulsions were then exposed, during several hours, to radiation at very high altitudes of the atmosphere from balloons and space crafts. Since the mid-fifties, there were from time to time reports on "heavy-nuclear cascades" with anomalously short mean free paths (mfp, λ) observed in cosmic ray interactions (1-7). Also, one publication reported the absence of this effect (8).

In 1980, the first accelerator-based experiment on this subject was performed at the Berkeley Bevalac, using ^{16}O and ^{56}Fe beams of ~2 A GeV (9), and anomalously short mfp's with $\lambda \leq$ "a few centimeters" was reported. Several more were to follow in the next few years, reporting mfp's in the range of $1 \leq \lambda \leq 6.5$ cm and with contributions of 2-15% of the total amount of fragments produced in the heavy ion reactions. There were, however, also a few reports from experiments where this effect was absent. Not only nuclear emulsions were used as detectors, but also other detector techniques like bubble chambers, plastic detectors and Cherenkov detectors. These detectors suffer from some general limitations. The lowest charge that can be separated is Z=10 in a Cherenkov detector and Z=7 in a plastic detector. In a bubble chamber Z>2 can not be separated and the events have to be classified into different topologies.

Several theories were proposed from which the anomalous behaviour could arise e.g. quark-gluon effects, color polarization of quark states, quasi-molecular states, nuclear density effects and metastable nuclear states. In the autumn of 1984, at the conference at GSI, Darmstadt in Germany (10), a survey of results from "anomalon" experiments were given. A status report (11) showed 33 sets of experimental data using different detectors and beams, all having a bombarding energy of a few A GeV. Out of these, 18 saw the effect and 15 did not. Table 1 shows a summary of these, where the different experiments have been sampled in 3 sets, depending on the amount of data gathered for the specific charges. There seems to be a strong

signal for anomalous fragments in the set with the lowest statistics, despite the ambiguity of the way data has been divided. In order to measure an anomalously short mfp, one must divide the data into bins of distance from the preceeding interaction, and this has been done in the same way in all the experiments listed. But, further division of the data into subgroups of different topologies may influence the sets given in the table by lowering the statistics, thereby shifting them into a set of lower number of interactions.

no. of secondary interactions	Anomalons	No Anomalons
< 1000	13	2*
1000 - 2000	4	4*
> 2000	1	9

Table 1. Experimental results of anomalous behaviour in different statistical bins.

Today, the quest for "anomalons" has subsided, and it has not, as yet, been possible to firmly establish if they exist or if they are the result of statistical fluctuations, biased estimators, systematic errors etc. Two papers on this subject are presented in this thesis. The first of these deals with a nuclear emulsion experiment and its position in the table above has been denoted by asterisks. The second paper covers a Monte Carlo simulation program (presented in section 2), developed to investigate the effects of low statistics in the interpretation of this type of experiments. The preference of finding anomalons in low statistics experiments, which seems to be at hand here, can however not be explained from the results of the simulation.

In this thesis, I will not discuss any of the above mentioned theories offered to explain an anomalous behaviour, since no anomalons were found in our experiment. A rather recent publication on the status of anomalons can be found in ref. 12.

1.1 Nuclear emulsions

The chemical composition of a nuclear emulsion is mainly silver halide crystals embedded in gelantin and water. Silver halide crystals are photo sensitive, i.e. they absorb energy from moving charged particles, thereby forming a latent image. When the nuclear emulsion is developed in a chemically reducing agent, the silver halide is converted to metallic silver, making the latent tracks from the passing particles visible in e.g. a microscope. In a standard emulsion experiment tens or hundreds of thin layers (pellicles) are packed close together to form a stack. This is irradiated, normally horizontally to the accelerated beam.

If a particle collides in the emulsion, each charged particle emitted in the collision leaves a secondary track. If the collision is reasonably central (and, of course, the energy is high enough), they will form a "star" of tracks going out in all directions from the collision point. The pellicles are re-aligned after developement, so that a track leaving one pellicle is easily found in the next for continous scanning in the microscope.

The mean energy loss per unit length is given by the Bethe-Bloch formula

$$J = C \cdot \frac{Z^2}{v^2} \cdot \left(\ln \frac{2m_e v^2}{I(1-\beta^2)} - \beta^2 \right)$$

where C is a constant depending on the composition of the absorber, Z is the charge of the particle and $v=\beta c$ its velocity. I is the mean ionization potential for the absorber and m_e is the electron mass. This formula is valid for particles with $m \gg m_e$. (A correction for interactions with atomic electrons and another for the polarization of the electric field for a relativistic particle has been omitted in the formula). The energy loss is therefore depending on both the charge and the velocity (energy) of the particle. Fig. 1 shows schematically the energy loss, J, as a function of β. At low velocities $1/v^2$ is the

dominating term. At very high velocities (β~1), J will mainly vary with the logarithmic term, which could also be written as const.*ln p (p is the momentum of the particle). Therefore, the mean energy loss will also slowly increase when β→1 and a minima will occur at β~0.96, marked in the figure as the point of minimum ionization. Above this limit the effect due to the polarization of the electric field mentioned above sets in, which decreases the effective range of ionization and therefore contributes to the increase in J.

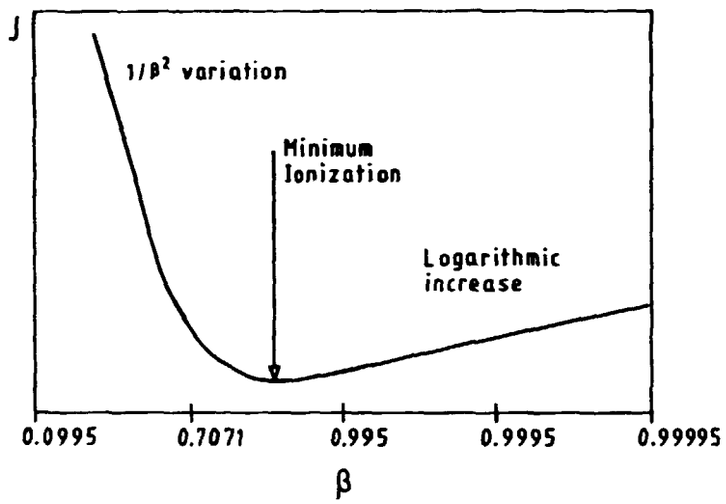

Fig. 1. Mean energy loss for a charged particle.

One parameter which can be measured experimentally is the grain density (gd), which for a fixed Z decreases with increasing velocity (energy) up to the point of minimum ionization. Due to saturation of gd at low velocities and high Z, one normally measures instead the gap density between the grains (blobs) or the gap length distribution, since the gap density is a parabolic function of the ionization. In order to determine both charge and energy, one must also measure either the range of the particle or the gradient of the ionization parameters. Other possibilities of charge determination are obtained with photometric measurements of track widths when β is constant, or profile measurements when β is varying.

1.2 Experimental details

The emulsion stacks were, for calibration purposes, also exposed to a low flux of ^{12}C. The sensitivity of the stacks was low (7 grains/100 μm), i.e. minimum ionizing particles with charge Z=1 were observed only with difficulties, and we must therefore assume a scanning loss of interactions where $\Delta Z \leq 1$. However, these losses were estimated from former experiments to be less than 2%. The advantage of the low sensitivity was an easier scanning for interactions and a better Z resolution in the photometric measurements.

The result of our experiment is based on 4370 fragments (902 interacting) of Z=2 and 2595 (1270 interacting) of Z=3-18. Beam tracks (6349) were followed "along the track", starting 3 mm from the edge of the stack to avoid possible mechanichal distortions near the edges. Also, 10 mm of each side of the stack was excluded from the primary scanning, since projectile fragments produced close to one side have a high probability of leaving the stack too soon after the collision, thereby making it hard to get a good charge determination. Primary interactions were only registered in the first half of the stack length (10 and 7.5 cm's respectively), leaving the rest to secondary and higher interacting generations, which were followed until either stopping or leaving the stack. Projectile fragments were identified as high energy particles (with $dE/dx \geq 4(dE/dx)_{min}$) emitted within a forward cone of $\theta \leq 10°$.

1.3 Determination of projectile charges

Charge determination was performed with two different methods. The part of the data handled by the Lund group (~50%), was measured by gap density and photometric measurements (13) of track widths. The gap density method is best suited for fragments with low charges, therefore the heavier ones ($Z \geq 5$) were determined by the photometric method. A photometer mounted on a microscope measures transmitted light from three parallel slits in a given field of view. The track to be measured is placed along the middle slit, and the background signal measured in the other two slits is subtracted. All charges were measured with 50 readings (totally 3.5 mm) starting at the production

point. Tracks too short for photometric measurements, or tracks passing local disturbances in the emulsion, were charge-determined by gap density measurements. This was performed for approximately 5% of the tracks.

The transmitted light is not only a function of the charge and its energy (track width), but it is also depending on the depth position of the track in the emulsion plate. The depth dependence of the transmitted light was therefore determined from measurements of beam tracks, and a correction term was calculated for each emulsion plate.

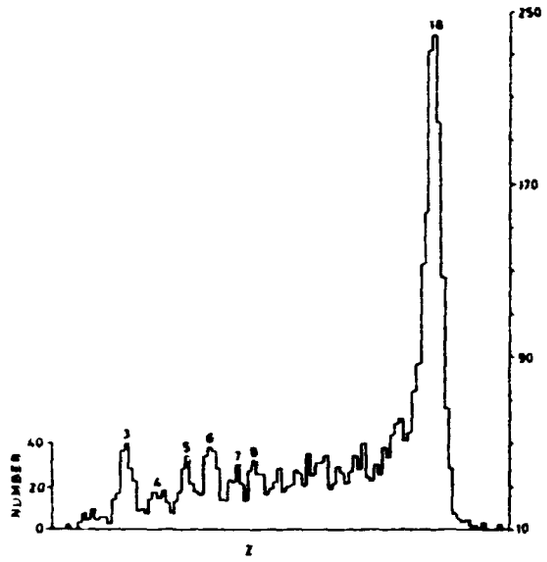

Fig. 2. Charge spectrum for projectile fragments from 1.8 A GeV ^{40}Ar ions.

The track width dependence of Z was determined for charges Z=6 and 18, as well as $2 \leq Z \leq 5$ (where Z is well determined by gap density measurements) and a fourth degree polynomial was then fitted to these points. Fig. 2 shows the charge spectrum derived from gap density and photometric measurements.

In the other half of the data, measured by our collaborators in India, charges were determined by gap length and gap density methods

only. This is described in ref. 14, where the different methods are compared, and found to be in good agreement with each other.

1.4 The Mean free path estimator

An anomalously short reaction mfp may be estimated by comparing mfp's measured for different bins of distance (usually 1 cm) from the preceeding collision. The mfp is normally estimated as $\lambda=s/n$, where s is the sum of track lengths scanned and n is the number of interactions found for a specific charge. This estimator is however biased for low statistics (15) and we have therefore used the less biased estimator $\lambda=s/(n+1)$, as suggested by (16), when determining the mpf for charge Z=2. The rest of the charges (Z=3-18) were combined with the charge independent parametrization $\lambda=\Lambda\cdot Z^{-b}$ in order to enhance the statistics. The behaviour of the two estimators and the parametrization of mpf's will be discussed in section 2.4. Experimentally we found $\Lambda=24.1\pm1.2$ cm and $b=0.34\pm0.03$, based on all our data, i.e. 6349 beam particles Z=18, 4370 particles of charge Z=2 and 2595 of charges Z=3-18. This is consistent with values found in other experiments, where normally Λ=23-35 cm and b=0.32-0.45. By using all our data, we have also included the possible anomalons, which might influence our result. However, two other experiments have found very similar parameter values with $\Lambda=25.1\pm1.7$ and $b=0.34\pm0.03$ (17), and $\Lambda=23.3\pm0.8$ and $b=0.32\pm0.01$ (18). In the first one, "anomalons" were found but in the second they were not, which shows that this is not crucial for the conclusion.

1.5 Sources of error

Sources of error must carefully be considered when estimating small effects like the one we search for. Inhomogeneities in the emulsion may induce variations in sensitivity, that can lead to misidentifications in the charge determination. Tracks found in observed inhomogeneity regions were therefore not charge determined in such areas. Another possible source of error is different scanning efficiencies for different observers, which has been checked by e.g. comparing the individual mfp's for primaries. As mentioned above, the low sensitivity in the emulsions leads to a loss of interactions with $\Delta Z=1$, and this was estimated to be less than 2%. Collisions from n, p,

d and t induced reactions may appear close to a track, and thereby be mistaken for an interaction. In an estimation described in paper 1, this effect is estimated to be as high as 20% for Θ_{frag}=0°. Later, the effect was introduced into the Monte Carlo simulation (paper 2) with more realistic fragmentation angles, and this reduced the effect to a mean value of 21 events in an experiment with our statistics. There also exists the possibility of misidentifying a low energy Z=1 particle with a more energetic one with higher charge (most probably Z=2), if the available track length is too short. This has been estimated to give one misidentified fragment per 600 in the first cm bin, increasing the mfp in the first cm bin with at most 1-2% (14).

2. MONTE CARLO SIMULATIONS OF ANOMALON EXPERIMENTS

The search for "anomalons" inspired us to develop this simulation program. When investigating such an effect, with no other obvious characteristics than an anomalously short mfp, this naturally requires a large enough amount of data in order to draw a statistically valid conclusion. We were therefore especially interested in how the statistical variance for e.g. the mfp estimator changed with the amount of data collected. At first, simulations were performed under normal conditions, and later anomalous fragments were introduced and the results were compared.

The simulation was constructed from well known empirical formulae whenever possible. It was, however, necessary to parametrize some of the variables included. Since we wanted to compare simulated results directly with experimental data, we choose the same statistics and the same detector size and volume of acceptance for beam projectiles, as in the experiment.

2.1 General computer scheme

When constructing a Monte Carlo program, it is important that the simulation agrees with reality as far as possible. If there are disagreements, one must investigate how these affects the final results. Also, all parts of the program have to be carefully checked, both individually and as a whole. The random generator is an important part and it must give uniformly distributed and non-repetitive random numbers. The random sequence is commonly initiated by a start number (seed), which has been taken from the computer clock in this simulation. Since a Monte Carlo program easily tends to become CPU consuming, attention must also be paid to avoid unnecessary loopings.

In this simulation, three main loops are entered, where the first one runs over the number of simulated experiments desired. The second deals with the number of beam particles to be produced, and the third and inmost one creates all projectile fragments in all generations possible to follow within the detector. (Fragments are commonly referred to as belonging to the first, second and so forth generation,

in order to denote at what stage in the reaction chain they have been produced). All projectile fragments, except those with charge Z=2, are then allowed to interact.

For each of these three loops, data has been collected and stored in different vectors. These have all been temporary, except those in the loop running over the number of simulated experiments. At the end of the simulation, most data which has been gathered are stored in histograms for output. When simulating the higher statistics experiments, the simulation had to be performed in smaller sequences, due to the increased execution time. In this case, all the data from one sequence was added to the earlier data stored on a data-file in the computer.

2.2 Particle production

The collision depth for all charges was taken from the collision probability $P(l)=1-\exp(-l/\lambda)$ which gives $l=\lambda \ln(1-P(l))$. The mfp (λ) was parametrized according to $\lambda=\Lambda \cdot Z^{-b}$, with $\Lambda=27.49$ cm and $b=0.409$. These values were taken from a preliminary evaluation of data and are therefore not the same as the values given in paper 1. A slightly different parametrization is, however, of small importance and therefore these parameters were used for all the simulations.

The empirical data on fragmentation was taken from ^{16}O, ^{40}Ar and ^{56}Fe (with beam energies of 2.0, 1.8 and 1.7 A GeV respectively). In some of the data, charge determination of projectile fragments had only been performed for Z=2. Therefore, data was sampled into fragmentation channels of (N_α, N_{Fr}), where the charge for N_{Fr} is ≥ 3. Fig. 5 in paper 2 shows some of the fragmentation channels extracted from the data. When constructing the fragmentation channel probabilities (see table 1 in paper 2) for all projectiles Z=3-18, these had to be extrapolated for projectile charges Z<8 due to the lack of data below this charge. For most of the channels, this was easily done because of the natural limitation of available charges in the vicinity of Z=8, e.g. the probability for the channel (4,0) would have to be zero for projectiles with Z<8. For the fragmentation channels (0,0) and (1,0) it was, however, not so simple since the

probabilities were both very high and still increasing for projectile charges below Z=8. Points for Z_{Fr}=2, obtained from α-projectiles in the ^{40}Ar data, were therefore used for guidance (also shown in fig. 5, paper 2). The channel probabilities for each projectile charge were then taken by vertically reading the (normalized) probabilities for the available channels. Channels with $N_{Fr}>3$ were omitted because of their small probabilities (0.002-0.007 for ^{56}Fe).

2.3 Charge distributions for projectile fragments

To construct the charge distributions needed for projectiles with Z=3-18, we used spectrometer data, Silberberg-Tsao's semi-empirical formulae for fragmentation cross-sections (19) and the experimental charge distribution for ^{40}Ar in emulsion. A nuclear emulsion mainly consists of ^{1}H, ^{12}C, ^{14}N, ^{16}O, ^{80}Br and ^{108}Ag targets, with the abundance of 0.22, 0.16, 0.04, 0.12, 0.22 and 0.24 respectively. The spectrometer data covered Z-distributions for ^{1}H, ^{12}C, ^{64}Cu and ^{108}Ag targets and therefore the ^{80}Br distribution was interpolated between ^{64}Cu and ^{108}Ag. For C, N and O targets, we used the carbon data.

The projectiles used in the spectrometer experiments were ^{12}C, ^{16}O and ^{56}Fe (with bombarding energies of 2.0, 2.0 and 1.9 A GeV). Fragmentation cross-sections for $Z\leq 12$ fragments in the ^{56}Fe case were not measured and therefore we calculated them from the following formula of Silberberg-Tsao,

$$\sigma(A_F,A_T) = \sigma(A_F,1) \cdot f(A_F,A_T), \text{ where}$$

$$f(A_F,A_T) = \begin{cases} 6\, e^{-2(A_T/A_F)} & \text{for H, C, N, O} \\ (1.6+0.07A_T^{2/3})\,(1-0.02A_F^{2/3})\, e^{0.02(A_F-A_T)} & \text{for Ag, Br} \end{cases}$$

where A_F is the fragment and A_T the target mass. A general parametrization was then performed with a simple polynomial fit for each emulsion target. Curves for ^{40}Ar for the case of CNO-targets are shown in fig. 3.

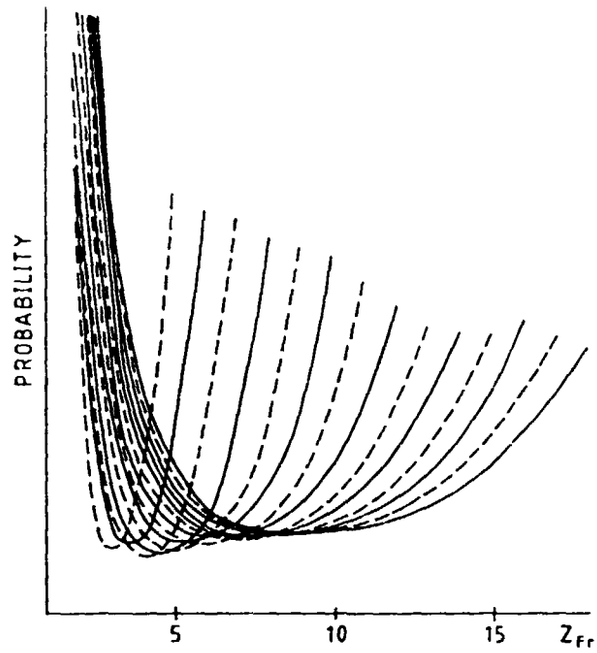

Fig. 3. Probabilities of charge distributions for projectiles with Z>4, produced in collisions with C, N or O-targets in emulsion.

Fragment charges for N_{Fr} in all multifragmentation channels (N_α,N_{Fr}) were drawn from these curves with the restriction of $\Sigma Z_{Fr}+2N_\alpha \leq Z_{Proj}$. Since the inclusive experimental charge distributions available normally include all possible fragmentation channels, this leads to a bias. With a projectile of charge Z=18, only the channel where no α particles are emitted (0,1) will draw a fragment charge from the whole interval available (3-18), whereas e.g. (2,1) will always draw a fragment charge in the interval of Z=3-14 due to the restriction mentioned above. This gives a suppression of the higher charges. An attempt to compensate the higher fragment charges for this decrease was made, and a formula for this is given in paper 2. It can, however, be written more compactly and I will here give an alternative expression:

$$f'(Z_F) = \frac{f(Z_F) \cdot C}{\sum_{N_\alpha=0}^{max} P(N_\alpha, Z_F)} ,$$

where

$$P(N_\alpha, Z_F) = \begin{cases} W(N_\alpha,1)/(Z_B-2-2N_\alpha) & \text{for } Z_F+2N_\alpha \leq Z_B \\ 0 & \text{for } Z_F+2N_\alpha > Z_B \end{cases}$$

Here, $f'(Z_F)$ is the compensated value of the inclusive distribution $f(Z_F)$ and C is a normalization constant. $W(N_\alpha,1)$ is the probability for the appropriate channels with $N_{Fr}>0$ (given in table 1 in paper 2). The probabilities for channels with $N_{Fr}=2$ has been added to the corresponding probabilities for $N_{Fr}=1$ in this calculation.

This correction (shown as open circles in fig. 4 in paper 2) was, however, not good enough. This could be due to the inclusion of $N_{Fr}=2$ probabilities in the $N_{Fr}=1$ weights, instead of treating them separately. We therefore solved the problem simply by drawing charges from a flat charge distribution, and determining the correction factors for each Z_F from the resulting distribution. Thus, the corrections included all possible multifragmentation channels with $N_{Fr}>0$.

2.4 The estimators

The two charge-dependent estimators $\lambda=S/n$ and $\lambda=S/(n+1)$ (for charge Z=10) are compared (see fig. 8 in paper 2) to the curves derived from the analytical expressions of $\langle\lambda\rangle$ given by ref. 15 and 16. The bin width is 1 cm and the comparison is made for the first bin after the collision. The simulated points follow the curves very closely, thus confirming the estimator problem for a low statistics experiment. This may further be seen as a measure of the accuracy of the simulation, showing that the parameters used, could reasonably well approximate an emulsion experiment.

The charge-independent mfp λ/λ_0 is (also in fig. 8) plotted against N, which may be confusing since we are here dealing with the charge-dependent estimators. The calculations and simulations have been performed for λ, but since this behaviour is similar for all charges, we have chosen to plot the results normalized to unity, i.e. λ/λ_z which perhaps would have been more appropriate to put on the y-axis. I would also like to point out that N here stands for the number of tracks with Z=10 found in the interval. Normally, in an experiment, the number of colliding fragments (n) are measured, which are approxi-

mately a factor of 10 lower than N.

In a high statistics experiment, the number of fragments found will decrease as shown for Z=10 by the arrow in fig. 8 in paper 2, assuming that the estimators show the same behaviour in all bins preceeding the collision. Assuming approximately the same behaviour for the charge--independent estimator, the decrease in N is shown for the sample of $3 \leq Z \leq 18$. It has, however, been shown by Lyons and Gibaut (ref. 20) that this is not the case. They also show that the mathematically equivalent expression for Λ,

$$\Lambda = \frac{\Sigma \lambda_z \cdot n_z \cdot z^b}{\Sigma n_z} = \frac{\Sigma S_z \cdot z^b}{\Sigma n_z}$$

gives completely different results. This is due to the fact that all events with $n_z=0$ will be excluded in the first expression, but not in the second (S_z). It will therefore bias the results, since the nominator remains the same in both cases (assuming that the same set of tracks are used in the calculation of Λ). The second expression is the most commonly used, and it was used in paper 1 and 2. As an illustration, fig. 4 shows its variation in 1 cm bins for N=100, 200 and 1000. The increase of Λ/λ_0 with increasing x is clear, even if the fluctuations are large for N=100 and 200. This rise is due to the decrease of N when x increases. This is a general behaviour, which is also mentioned in the next section, giving a broader and flatter distribution of Λ.

The fact that Λ/λ_0 always is above the expected value is also following from the effect of events with $n_z=0$ being excluded. When the number of fragments decrease, these events are being unduly favoured (to what extent is of course depending on the probability of finding $n_z=0$), since the probability of finding a collision will always be smaller (~ one order of magnitude as mentioned above). When using the first expression this behaviour will be reversed, and the mfp estimator will in consequence decrease with N. Therefore, also the charge-independent mfp estimator is biased when $N \to 0$, but the behaviour

is not comparable to that of the charge-dependent estimators.

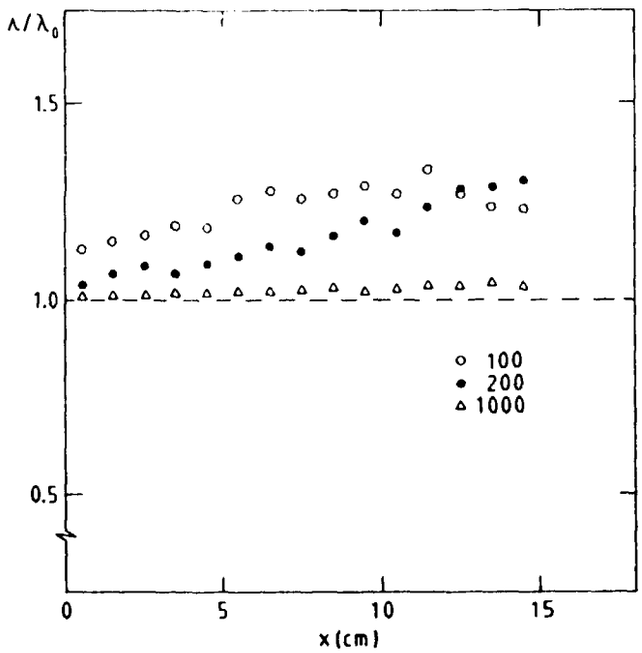

Fig. 4. Variation of the charge-independent mfp estimator with distance from the collision point (bin width 1 cm).

2.5 General results

We have compared the distributions of the charge-independent mfp estimator for different numbers of colliding beam particles. In paper 2 we show the distributions obtained from the simulation of 600 experiments with 3000 and 600 colliding beam particles respectively. The bin size is 1 cm and the distributions have a gaussian shape for the first cm's in the high statistics case. They are, however, Poisson-like already in the 4:th cm bin, with an extended tail on the $\Lambda/\lambda_0>1$ side. This is due to decreasing statistics, since the number of collisions (and fragment tracks) encountered decreases when moving further away from the collision point. If the bin size is increased (which is usually done for the later bins) to e.g. 2.5 cm, the statistics will increase, thereby shortening the extended tail. For the case of the lower statistics, the distributions in consequence become even

more extended, and therefore flattened.

When an anomalous component is introduced, the expectation value of Λ/λ_0 is of course shifted downwards (the mfp for anomalons is taken to be λ=2.5 cm). In the high statistics case, the 6% anomalon distribution is clearly distinguishable in the first bin, but for increasing x it approaches the non-anomalon limit. Due to the extended distributions in the low statistics case, it here overlaps the non-anomalon distribution with 53% as compared to 18% for high statistics, which can be seen in fig. 11 and 9 in paper 2. Our conclusion is therefore that a 6% component would most probably be seen in an experiment with at least 3000 colliding beam particles, whereas for experiments with low statistics, such a contribution can not be significantly distinguished from a non-anomalon distribution. As for the case of a 2% anomalon component, it is not distinguishable even with the higher statistics.

The reaction chains shown in the first reports on "heavy nuclear cascades" (1-3) were short, and when other short chains were reported it was suggested that the anomalous behaviour would remain even after a collision had occured. This "memory"-effect was also simulated. The available length, and thereby the lengths of the reaction chains, is of course depending on the size of the detector. Therefore, the detector-size and experimental data were taken from the Lund stack. (A simulation was also performed for the other stack, with comparable results). The non-anomalon simulation is in good agreement with the experiment, however not quite within the errors. This could e.g. be due to the higher Λ, improper weighting of the fragmentation channels or too high probabilities for heavy charges in the parametrization of the charge distributions. This is however of no importance for our conclusions on the 6% "memory"-effect, where the reaction probability is strongly enhanced and is clearly seen already in the third link of the reaction chain. Even so, we conclude that it would be difficult to observe even such a strong memory effect experimentally, due to the large statistical errors in the later stages of the reaction chain.

2.6 Sources of error

Systematic errors in the simulation will, of course, affect our results. It is therefore important to know how much they will be affected, and if this will influence our conclusions. The generated reaction chains, mentioned above, are most strongly influenced by systematic errors, partly due to the limited detector size. In addition to the parameters already mentioned, also the collision probability P(1) (which is also depending on λ, see section 2.2) and the fragment emission angle may cause systematic errors. These will individually lead to both shorter and longer chains, but taken all together they may extinguish each other. Therefore, both wider emission angles and the extreme case of a flat charge distribution were introduced, neither leading to any change in our conclusions for the reaction chains of the mfp estimators. The error of "low energy" Z=1 fragments, discussed in iii) in paper 2 has already been mentioned in section 1.5.

The estimation of "confusing" Z=1 and neutron induced reactions (discussed in iv) in paper 2) has been simulated. In each reaction, 2/3 of the residual projectile charge remaining after the randomization of projectile fragments was emitted, in a narrow forward cone as singly charged particles. For all fragment tracks in the reaction chain, collisions from such "confusing" particles were investigated. If a reaction from a "confusing" particle appeared within 10 μm of a fragment track, it was considered as a misidentified collision. In the simulation, a mean number of 21.9 "confusing" singly charged particles were produced in each primary collision. From these, there were 137 misidentified collisions in $2 \cdot 10^4$ primary collisions, thus giving approximately 21 misidentified collisions in a high statistics experiment.

3. "SUBTHRESHOLD" PION PRODUCTION

A prediction of the existence of the pion came already in 1935 when H. Yukawa developed a field theory of the nuclear force, where the pion was the field quanta in analogy of the role of the photon in the theory of electromagnetic fields. It took, however, another twelve years before the existence of the pion was confirmed in a cosmic ray experiment, using nuclear emulsions which were exposed on mountain tops (21). Pion production in proton induced reactions was studied already in the early fifties, whereas studies of pions produced in heavy ion collisions could not be systematically studied until the seventies.

In order to explain the expression "subthreshold", I will briefly discuss some thresholds to be encountered. The highest one is the threshold to produce a pion in a free nucleon-nucleon (NN) interaction. From relativistic kinematics this threshold is given by

$$\varepsilon_{th} = (m_\pi{}^2 + 4m_N m_\pi)/2m_N$$

(m_π is the charged pion and m_N the nucleon mass), which requires 290 MeV.

If the colliding particles, on the other hand, are inside two nuclei, their internal (Fermi) momentum vectors will be added to the relative momentum, thereby possibly lowering the threshold of energy required to produce a pion. With F_1 being the incident and F_2 the target nucleon Fermi momentum, the threshold is then given by

$$\gamma^{th}_{inc+F_1} \cdot \left(1+\beta_{F_2}\cdot\beta_{inc+F_1}\right) = \frac{0.5[2+(m_\pi/m_N)]^2 - 1}{\gamma_{F_2}}$$

Here, $$\beta_{inc} = \frac{\beta^{th}_{inc+F_1} - \beta_{F_1}}{1 - \beta^{th}_{inc+F_1}\cdot\beta_{F_1}}$$

and with the threshold given by $\varepsilon_{th} = (\gamma_{inc} - 1)m_N$

If we use the standard Fermi momenta for nuclei in their ground state, the threshold will now decrease to ~42 A MeV for a light symmetric system (C+C) and ~30 A MeV for a heavy asymmetric system (C+Pb).

If the pions on the other hand are produced in a totally collective process including all nucleons in the nuclei, the threshold will be further lowered, and will be given from

$$\varepsilon_{th} = (m_\pi{}^2+2(A_1+A_2)m_N m_\pi)/2A_2 m_N$$

(A_1 is the mass of the incident nucleon and A_2 is the target mass), which gives approximately (binding energies are neglected) 23 A MeV for C+C and 12 A MeV for C+Pb.

The simplest classical NN model assumes first-step NN scattering with sharp Fermi-spheres and Pauli-blocking (22). Results from such calculations strongly underestimate the pion production cross-section, as shown in fig. 3 in paper 4. An extension of this model, assuming soft Fermi-spheres, was made (23) but the theoretical cross-sections were still too low. Allowing interactions between clusters of nucleons, one comes close to the cross-sections (24). Completely collective models like pionic fusion (25) and nuclear bremsstrahlung (26) have also been suggested. These models are indeed succesful in explaining the data even if the underlying physics is not obvious.

3.1 The experiments

The first accelerator-based heavy ion experiment to measure production cross-sections for "subthreshold" pions was reported in 1979 by Benenson et al. (27). It was performed at the Bevalac with an 80 A MeV beam of Ne on NaF. The CERN synchro-cyclotron (SC) was at the same time upgraded, and in 1980 it could produce slowly extracted ion beams with high intensities, well suited for pion production studies. The ^{12}C beam, which we have used, could exhibit a current of 20 nA on the target with a duty factor of about 30%. Thus, the Bergen-CERN--Grenoble-Lund-Saclay collaboration decided to start a program on "subthreshold" pion production. All three experiments on this subject

that are presented in this thesis (paper 3-5), were performed at this accelerator during the years 1981-1986.

Normally, the full energy - 85 A MeV - was utilized, but a degrading of the beam down to 60 A MeV was made in the second experiment (1984). This was in fact the lowest energy where pions had been measured at that time. In the first two papers presented here, only inclusive pion measurements were made, whereas in the last paper additional coincidence measurements of charged particles in the forward direction was performed. Table 2 gives a summary of targets, angles etc. from these three experiments.

Beam energy A MeV	Intensities ions/s	Targets	Angles degrees
85	$(2\text{-}25)10^9$	C, Au	55, 90, 130, 145
85, 75, 60	$(5\text{-}10)10^9$	Li, C, Pb	27, 60, 90, 120
85	$(0.1\text{-}0.4)10^9$	C, Sn	70

Table 2. Summary of experimental set up for papers 3-5.

In the first two experiments we used thinner targets (50-100 mg/cm^2) than in the last experiment (113-190 mg/cm^2). In the former, an average beam energy loss in the targets of <2 A MeV was estimated. In the last paper, the decrease in the effective beam energy is estimated to be about 2 A MeV for C+C and 3 A MeV for the Sn targets.

3.2 Pion detection

In all pion experiments presented here, plastic scintillator range telescopes were used for pion detection. Such a telescope consists of scintillators placed after each other. The thickness of each scintillator is adapted to the desired energy-loss. Thus, each element corresponds to one pion energy bin, and no further energy calibration is done for a range telescope.

The low energy detection limit for the pions is set by the need to use a number of elements in the front to confirm that a "true" particle has entered the telescope. Normally, at least one element at the end is used only to register particles passing through, i.e. to act as a veto detector. The upper energy limit of the pion detection is, however, set by the loss of pions due to nuclear reactions in the detector material (fig. 2 in paper 5). The loss of 80 MeV pions will be ~40%, and this must be regarded as a practical upper limit due to the loss of pions.

Limitations in the angular position exist in the forward direction due to the increased flux of the fast protons, which must be rejected with a high enough efficiency in order to isolate pions. The eventual large angle limit is set by the decrease in the pion production cross-section itself.

The range telescopes are constructed from plastic scintillators. One advantage of plastic scintillators is their fast response (the rise time of the pulse is a few nanoseconds, which is important for measuring the decay of the positive pion, τ=26 ns). Details about electronic setups may be found in ref. 28 (paper 3 and 4) and ref. 29. The data acquisition was based on CAMAC readouts in all three experiments. In the last experiment, we have used an additional CAB system, where further particle rejection was made on-line in the CAB-processor, thereby substantially increasing the on-line rejection.

3.3 Pion identification

A selective hard-ware trigger is essential in these events, when only a very small fraction of the detected particles are really pions. The positive pions are identified with two different methods - the TDC and ADC method, both based on the decay of the positive pion $\pi^+ \rightarrow \mu^+ + \nu_\mu$. The mean life time of the pion is 26 ns, and the kinetic energy of the μ^+ is 4.2 MeV.

Due to the fast recovery time (18 ns) of the electronics used in these experiments, it is possible to measure two different time

signals, the prompt (the pion itself) and the delayed time (the occurence of the muon). The prompt TDC is started by the acceptance of a "true" particle and stopped by a signal from the stop detector. If no signal is found in the preceeding detector, the delayed TDC will be stopped by the emitted muon. The TDC method was used in papers 3 and 4 (described there as method i)).

The ADC method, which was used in papers 4 (method ii)) and 5, is also based on strong on-line proton rejection and on the identification of positive pions from the delayed energy signal from the muon. Rejecting the strong proton background is a major task. The energy deposit (ΔE) from most protons passing through a detector is higher than that from a passing pion. Therefore, discriminator levels were set in all detectors. A stopping particle was then rejected if the ΔE deposits in the preceeding detectors were found to be above this level. Also, an additional test for the ΔE-E position of the stopping particle was made by the fast CAB system in the last experiment, as mentioned in the previous section.

After accepting a stopping particle, the energy signals are integrated both within a prompt gate and a gate which has been delayed. If a muon was emitted from a decaying positive pion, an energy of 4.2 MeV would be added to the energy measured the delayed gate. This shift would be seen in the off-line analysis, when displaying the energy in the delayed gate versus the prompt for the stop detector (see fig 5b).

In paper 4 and 5, also negative pions have been measured. The slow negative pions interact strongly with nuclei, and they are therefore captured in the detector before having time to decay. An additional energy deposit will then come from the products emitted by the capturing nucleus. This energy deposit is "prompt", and can not be separated from that of the pion. Negative pions are accepted by the hard-ware since they have the same ΔE as positive pions, but they will not appear shifted in an off-line prompt-delayed energy plot. Thus, the number of negative pions can be determined from the difference between the total number of charged pions and the number of π^+

actually identified. Two ΔE-E plots for pions stopping in the fifth and seventh element of the range telescope are shown in fig. 2 in paper 4. In the right hand figures, the energy added to the negative pions is seen. (In the text below the figure it should be S_5 [(a),(b)] and S_7 [(c),(d)]).

The negative pions, measured in the second and third experiments are thus identified from ΔE-ΔE correlations in the off-line analysis. High energy protons may give ΔE signals similar to that of a pion, but they will be rejected if passing the veto detector(s) at the end of the telescope. However, if they have such a direction that they leave the telescope in an earlier element (which may occur for particles passing near the edges), they can not be separated from the negative pions. This effect was avoided in the second experiment by using a small front detector to ensure that protons passing this detector, also must pass the veto detector. Since the contamination of fast protons were considered to be small at 70°, a larger front detector was used in the last experiment in order to increase the solid angle. In the off-line analysis, however, it became evident that although the production cross-section is low for such fast protons, it is not negligible in comparison with the production of negative pions. This is why the error is substantially larger for the yield of negative pions in paper 5.

3.4 The fragmentation wall

In the last experiment, pions (and protons) were measured in coincidence with projectile-like fragments in the forward direction. These were detected with a front wall detector system with twenty-four ΔE-E detector pairs placed in two rings (see fig. 1 in paper 5). Also here, plastic scintillators were used. The pion range telescope acted as the trigger and all wall elements were read out (with no restrictions) each time a particle was accepted in the range telescope. The ΔE scintillators were thick enough (2 mm) to allow a good separation of the fragment charges Z=1-6. The E scintillators (80 mm) stop all particles except the highest energy Z=1 fragments. Fig. 3b in paper 5 shows an example of the charge resolution in the wall detectors.

3.5 Data analysis

The data analysis program was originally written for a Nord-100 computer, but in the beginning of the analysis of the last experiment, it was transferred to a VAX computer. To ensure that there were no inconsistencies, some of the earlier results were reanalysed on the VAX and found to be identical to those from the Nord-100.

The computer program is organized in menus, and handles all data processing. Since only a very small fraction of the events stored on tapes during the experiment are pions, the analysis was made in two steps. The first was to select the pion events and save these on disk files together with the wall readouts. In the second step, the wall data was analysed from these events. Within the analysis program, it is possible to display energy and time signals in histograms, and any combination of signals (both energy and time) can be displayed as bi-dimensional scatter plots. Areas may then be defined in these plots in order to select particles with desired properties like e.g. positive pions in a prompt versus delayed energy plot.

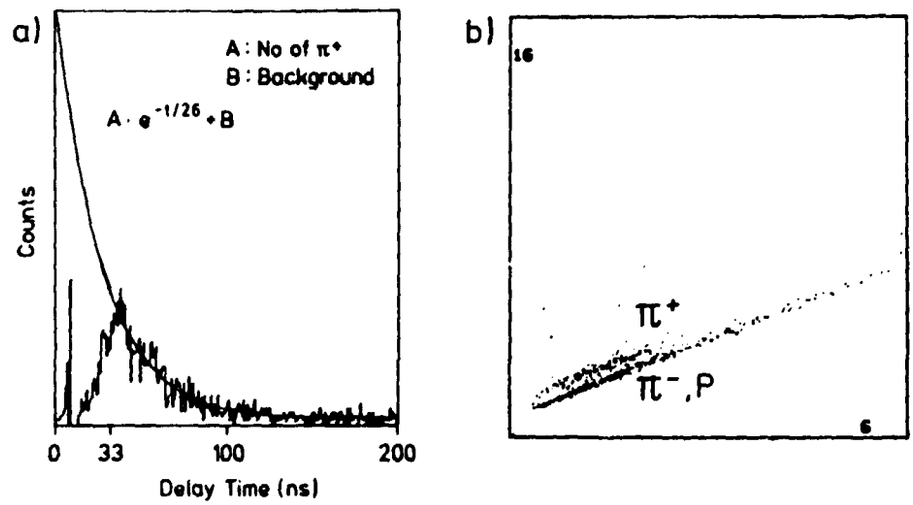

Fig. 5a. Decay spectrum obtained with the TDC π^+ identification method.

5b. Prompt versus delayed energy plot d or particles stopping in element b, obtained with the ADC π^+ identification method.

The positive pions have been identified by the two methods (TDC and ADC), described in section 3.3. Fig. 5a shows a typical decay spectrum obtained with the TDC method. The exponential decay curve is fitted in the interval of 33-200 ns. In order to obtain the number of positive pions stopping in the detector, this curve is extrapolated to t=0. The ADC method is illustrated in fig. 5b, where the delayed versus the prompt energy signal for stopping particles is displayed. The 4.2 MeV shift from the decay of the positive pions is clearly seen. The efficiency of this method has been estimated to 0.82 ± 0.05 (29) using a beam of positive pions.

Further software rejection has been made by cuts in the prompt time signal (see section 3.3). In this, random (background) particles arriving too soon/late are also removed.

Negative pions have been identified by first determining all pions with ΔE-ΔE area cuts in all detectors preceeding the stop detector, and thereafter subtracting the number of positive pions found. In consequence, the errors for negative pions are larger than those for the positive pions. In the last experiment, the contamination of fast protons was estimated from the π^-/π^+ ratio in the C+C reaction measured in paper 4.

The charges of the fragments measured by the front wall in paper 5 was also determined by area cuts in the ΔE-E plots. Due to small differencies in gain, each ΔE-E correlation had a slightly different position of these areas. An off-line multiplicative adjustment of the gains made it possible to apply the same area cuts on all ΔE-E correlations. The adjustments were made with the proton coincidence data, since these had the highest statistics. Due to the good charge resolution in the ΔE, the adjustments were not particularly crucial and therefore rather easily done. A cut in the coincidence time spectrum was performed for the fragmentation wall, which removed all particles with improper timing. After applying all area cuts for the projectile fragments, 21% of the positive pions remained for the carbon target. The corresponding figure for the tin targets was 11%.

3.6 General results

The doubly differential cross-sections for C+C for all experiments (compared in fig. 5, paper 5) are in good agreement with each other. Also, the slopes of the exponential fall-off is similar. A summary of production cross-sections as a function of beam energy is shown in fig. 6. The black dots are from our experiments, the open circles from ref. 27 and the triangles from ref. 30. All data above 100 A MeV comes from Ne+NaF collisions which have been scaled with $A^{(0.8)2}$.

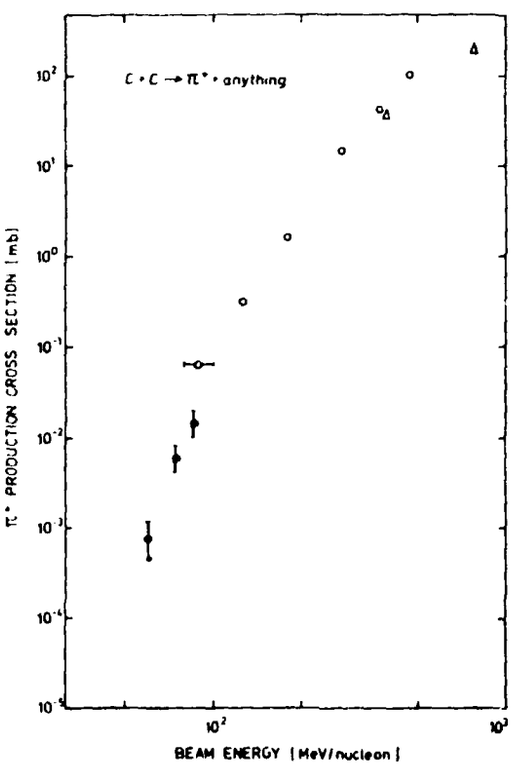

Fig. 6. Production cross-section for positive pions.

It is suggested from the A_T-dependence shown in paper 5 (fig. 8) that reabsorption is an important effect which has to be further investigated. The A_T-dependence straightens out considerably when applying the calculated escape factors (the probability for a pion to penetrate nuclear matter), and an over-all fit gives a slope around

α=1.0. In the low target mass region, a residue of the steeper slopes for large angles is indicated (see fig. 15 in paper 2). The significance of this is, however, difficult to estimate due to the spare amount of data and poor statistics.

The escape factor (see fig. 14b, paper 2) is low at forward angles for a heavy target, but increases when going towards backward angles. Thus an angular spectrum will be shifted towards more forward peaking when applying the reabsorption correction. This would e.g. shift the spectra in the NN c.m. system shown in fig. 2 in paper 3 towards less backward peaking, and it means that the original production system could be faster than first believed. The inclusion of reabsorption in first chance NN calculations, will however further decrease the final cross-sections and make them fall even more below the measured ones.

Both the A_T-dependence after correction for reabsorption and the suppression of high fragment charges in the front wall (paper 5) point towards pions being produced in central collisions. This certainly puts a new constraint on all models claiming to explain the bulk part of pion production.

The π^-/π^+ ratio has been measured for different reaction systems in paper 4 and 5. In the former, the energy shift between π^+ and π^- observed in the energy distributions for the isospin symmetric C+C (where $\sigma_{\pi^-}/\sigma_{\pi^+} = 0.62\pm0.19$) corresponds to the Coulomb shift from a compound-like nucleus. The $\sigma_{\pi^-}/\sigma_{\pi^+}$ ratio is 1.5 ± 0.4 for C+Li and 1.5 ± 0.3 for C+Pb, which is close to the (A-Z)/Z values of 1.33 and 1.54 respectively. However, applying a compound nucleus Coulomb shift to these systems will give a too large π^- excess to be explained by any reasonable neutron excess. In the Pb case it will be a factor of 7, and we therefore do not believe in applying a compound nucleus Coulomb correction.

In paper 5, the relative $\sigma_{\pi^-}/\sigma_{\pi^+}$ ratios for the two Sn isotopes are presented. In fact, the $\sigma_{\pi^-}/\sigma_{\pi^+}$ ratio for each isosope is in both cases close to 1.2, but with large errors due to previously mentioned problems in the π^- identification. The statistical model (with Coulomb

effects included) of Bonasera/Bertsch (31) gives a ratio for C+Pb which is in good agreement with that found experimentally. Also for the C+C system, the ratio is reproduced.

3.7 Perspectives

There are certainly still questions around "subthreshold" pion production that have not been answered. Our collaboration has planned a series of pion experiments at the CELSIUS storage ring at TSL, Uppsala (32), where the first heavy ion beam can be expected next year. One advantage of this accelerator is that beam energies can be rapidly changed. We therefore plan to measure pion production in nearly the whole range of beam energies shown in fig. 6, starting at 460 A MeV and step by step decreasing it to the lowest possible energy. The onset of new processes and possible anomalies may then be studied in this energy range in one single experiment, using the same beam-target configuration. For this experiment, three large solid angle range telescopes will be used for pion registration, and later on, projectile or target fragments can be measured in coincidence with the pion production.

As mentioned earlier, one of the drawbacks in studying pions is the reabsorption in the target nucleus. There has therefore been speculations of measuring subthreshold kaons as a probe for the situation in the interior of interacting nuclei. Due to the conservation of strangeness, their mean free path is long and they are therefore not reabsorbed in the target. However, kaons need of course higher collision energies, since their mass is 494 MeV/c^2 and they must be produced together with another strange particle. Furthermore, their mean life time (12 ns) is only half of that of the pion. Several problems in the detection of kaons can be foreseen, and the probabilities of doing subthreshold kaon experiments at CELSIUS is therefore an open question.

4. SUMMARY OF PUBLICATIONS

Paper 1. Search for Anomalous Fragments in 1.8 A GeV ^{40}Ar Reactions in Nuclear Emulsions

In this paper we investigate the existence of projectile fragments with anomalously short reaction mean free paths (mfp). The experiment was performed in collaboration with the Universities of Banaras, Chandigarh, Jaipur and Jammu in India. Our aim was to obtain a statistically significant conclusion by collecting the amount of data required to avoid biased results from the mfp estimator.

Two Ilford G5 emulsion stacks were irradiated at the Berkeley Bevalac with a beam of ^{40}Ar at 1.8 A GeV. A total of 6349 beam particles (primaries) were followed, giving 4370 particles with charge Z=2 and 2595 of charge Z=3-18 in the subsequent fragment generations. Much effort was devoted to charge determinations, which were made by photometric measurements and gap length or gap density determinations.

The most commonly used mfp estimator $\lambda=S/N$ (S is the sum of the track lengths for one charge, and N is the number of interactions found), is biased when statistics are low and it was therefore replaced by the less biased estimator $\lambda=S/(N+1)$. For charges Z=3-18, we used the parametrization of the mfp, $\lambda_z=\Lambda\cdot Z^{-b}$, in order to gather mfp data from all the different fragment charges. A combination of these give

$$\Lambda^* = \frac{\Sigma\, \lambda_z^* \cdot n_z \cdot Z^b}{\Sigma\,(n_z+1)} = \frac{\Sigma\, S_z \cdot Z^b}{\Sigma\,(n_z+1)}$$

The parameters Λ and b, with $\Lambda=24.1 \pm 1.2$ cm and $b = 0.34 \pm 0.03$ were determined from all our data. Λ^* and λ^* were determined for different bins of distance from the interaction point for the two subsamples with charges Z=2 and Z=3-18. Neither of these subsets exhibit any anomalous behaviour.

In a preliminary report with lower statistics data was sampled, by visual estimation only, into charge groups of He (Z=2), light (Z=3-5), medium (Z=6-9) and heavy (Z=10-18) charges particles. When plotting λ^* as a function of distance from the interaction point, there was a deviation of ~3 s.d. below the mean value in the first bin. We then decided to enhance the statistics for the first few centimeters, and also to determine the individual charges. When evaluating our final data, however, no deviation from the mean value of λ^* was found.

Two possible systematic error sources are discussed in this paper. The first is the "confusing" p, d, t and n induced reactions. It was estimated to be 20% in the first cm bin if all fragments were emitted with $\theta=0°$. The Monte Carlo simulation (see paper 2) shows that with the introduction of realistic fragmentation angles, this is reduced to a very small correction. The second error source is low energy fragments with Z=1 which give a dE/dx similar to fragments with $Z\geq 2$. Provided that the track length is short enough, they may therefore be mistaken for a higher charge and this error was estimated to ~3%. A few false collisions of these kinds were actually found and corrected for.

Paper 2. Monte Carlo Simulations of Anomalon Experiments

Observations of enhanced reaction probabilities (2-6%) for projectile fragments produced in heavy ion reactions with energies of a few GeV were reported. However, also some contradictory results were reported. This Monte Carlo simulation program was developed in order to examine the statistical fluctuations of the mean free path in experiments with limited statistics.

In the simulation, the detector size was taken from our emulsion experiment (paper 1), as was the charge of the impinging beam particle, ^{40}Ar. Projectile fragments were emitted within a forward cone of $\theta\leq 10°$, following a Gaussian transverse momentum distribution. The multi--fragmentation channels were constructed with parametrizations and interpolations based on the empirical data available, with a guidance

from Silberberg-Tsao's semi-empirical formulae.

The behaviour of the estimators $\lambda=S/n$ and $\lambda=S/(n+1)$ with the variation of N (which here stands for the number of tracks found) was investigated, and the simulated points do very well follow the curves derived from the analytical expressions of these estimators. It is clearly seen that the former estimator is more strongly biased than the latter, i.e. the deviation from the asymptotic mfp value sets in at N~500 for the former as compared to N~50 for the latter. A division of data into subgroups will lead to a decrease in the statistics, i.e. towards the biased part of the curve. When using these estimators, it is therefore advisable to enhance statistics until, at least a few hundred particles have been collected in each bin (subgroup). Also the common charge-independent Λ is biased, however not with the same behaviour.

We have also investigated the statistical width of Λ as a function of Δx (with a bin width of 1 cm) when anomalous components of 2 and 6% are introduced. With reasonably high statistics (3000 colliding beam particles, i.e. of the same order as in paper 1), we show that a 6% contribution should be significantly observable in the first few bins, whereas a 2% interference mainly falls within the statistical errors of a non-contribution. It is also shown that for a "low statistics" experiment (with ~600 colliding beam particles), not even a 6% contribution will be distinguishable. The "memory"-effect, leading to an enhanced probability of interactions in subsequent generations, has also been studied. When introducing a 6% component with full memory (anomalous behaviour throughout the reaction chain), the enhancement is clearly seen already in the third generation. The probability of obtaining a significant result in one single emulsion experiment is however small, due to statistical errors.

Possible systematic errors are finally discussed. In paper 1, the "confusing" p, d, t and n interactions were estimated to 20%. This was introduced into the simulation with more realistic fragmentation angles and was found to give a very small contribution.

Paper 3. Subthreshold Pion Production in Heavy-Ion Collisions at 85 A MeV

π^+ production was studied for $^{12}C+C$ and $^{12}C+Au$ reactions at 85 A MeV. The detector system was a range telescope, consisting of six plastic scintillators, giving an energy range of $20 \leq E_\pi \leq 80$ MeV. The telescope was placed at 55, 90, 130 and 145 degrees in the horizontal plane.

The doubly differential cross-sections show an exponential fall-off with increasing pion energy and they have similar shapes for both targets, with ~9 times higher cross-sections for Au. Furthermore, the slopes are getting slightly steeper with increasing laboratory angle.

The invariant cross-sections, $(1/p)d^2\sigma/d\Omega dE$, are compared for three different center of mass systems - nucleon-nucleon (NN) cm, nucleus--nucleus (nn) cm and laboratory frame. The spectrum for the gold target is slightly forward peaked in the nn cm and lab frame, but distinctly backward peaked in the NN cm frame. Since the spectrum in the nn cm system is closer to symmetry than in the NN system this would indicate a reaction mechanism with more than two nucleons involved. However, reabsorption of pions in the target nucleus could cause an asymmetry, a possibility which is further studied in paper 5.

If a power law target mass dependence ($\sim A_T^{\alpha}$) is adopted for the differential cross section, it would give $\alpha \sim 0.8$. The apparent temperature, observed in these reactions, are 14 ± 1 for C+C and 15 ± 1 for C + Au.

Paper 4. Production of Charged Pions in Intermediate-Energy Heavy Ion Collisions

Pion production below 85 A MeV is measured for a beam of ^{12}C on Li, C and Pb targets. Four identical, twelve element, range telescopes were

used in order to register pion cross-sections in a wide range of angles (27, 60, 90 120 and 150 degrees). The telescopes were designed to detect pions with energies of E_π = 27-82 MeV. The beam was also degraded to 75 and 60 A MeV for measurements of pion production in ^{12}C+C reactions.

The doubly differential cross-sections show the same exponential behaviour as found in paper 3. The π^+ cross-sections for C+C reactions were found to be a factor 3-4 lower at 75 A MeV and 10-20 lower at 60 A MeV, as compared to the cross-sections at 85 A MeV.

Positive pions were identified by their decay ($\pi^+ \rightarrow \mu^+ + \nu_\mu$), whereas negative pions were identified by ΔE-ΔE correlations in all detectors preceeding the stop detector. This introduces somewhat larger uncertainties in the π^- cross sections as compared to π^+. Comparison between π^+ and π^- spectra show a 10 MeV shift for the isospin symmetric C+C system, and this is interpreted as a pure Coulomb shift. By using (A-Z)/Z to calculate the isospin weights for the production channels, a ratio of 1.33 is found for Li and 1.54 for Pb. When compound nucleus Coulomb energy shifts are introduced, the experimental ratios for π^-/π^+ are found to be 1.8 for Li and 7 for Pb, which can not be explained by neutron excess in the target nuclei.

Angular distributions ($d\sigma/d\Omega$) are compared for laboratory and nucleon-nucleon (NN) cm systems. The spectra for all targets are forward peaked, which is becoming more pronounced with decreasing target mass. In the NN system, the light target data are still strongly forward peaked, whereas for the heavy target the peak is now at backwards angles. The spectrum with carbon is found to be approximately symmetric. Differencies in source velocities could explain these NN spectra, and this would imply that the production source is faster than the NN cm system for the light target, and slower for the heavy one. Also, the possibility of reabsorption effects are discussed to be a part of these discrepancies. The apparent temperature for C+C was here found to be 17 ± 2 MeV, i.e. within the errors the same as that given in paper 3.

Paper 5. Charged Pion Production and Projectile Breakup in 85 A MeV ^{12}C induced Heavy Ion Reactions

In this paper, a further step is taken towards understanding the nature of pion producing reactions below the free nucleon-nucleon threshold. By introducing a front wall for detection of projectile fragments in reactions where pions are produced, information on the impact parameter may be studied. A beam of ^{12}C at 85 A MeV was used in combination with C, ^{116}Sn and ^{124}Sn targets. The pion range telescope (nine elements, giving E_π=15.7-60.3 MeV) was placed at 70 degrees (horizontal plane) for all data collected. The fragmentation wall covered ~80% of the region $2.2° \leq \Theta \leq 7.0°$ in an arrangement of two rings with 2*12 ΔE-E plastic telescopes.

The inclusive cross-sections for C+C was found to be consistent with those measured earlier (paper 3 and 4). The apparent temperature has been settled from all our π^+ data to 15 MeV.

Isospin weights are estimated for the two tin isotopes. As was mentioned in paper 4, the errors for π^- cross-sections are larger than those for π^+ due to the indirect identification method. In this paper, the uncertainty is increased by a larger background of high energy protons and the error in π^- cross-sections are estimated to be as high as 25-30%. We have therefore chosen to compare the relative $\sigma_{\pi^-}/\sigma_{\pi^+}$ ratios of the two isotopes, which within the errors agree with the expected (A-Z)/Z ratios.

The target mass (A_T) dependence has been investigated for all targets used - including data from paper 3 and 4, i.e. Li, C, Sn, Au and Pb. When plotting $d\sigma/d\Omega$ against A_T, it becomes evident that the target mass dependence changes from the low A_T to the high A_T region and varies from angle to angle. The power α increases from ~0.6 (for 27° up to ~3.2 (for 120°) in the low A_T region. A transformation of the cross-sections to other production systems do not affect the slopes in any significant way. Thus our conclusion is that reabsorption in the target plays a dominant role. Escape factors for pions were therefore

calculated for different A_T, assuming central collisions and with a pion mean free path of 3.0 fm on the average. The escape factors vary both with the pion energy and the emission angle. When these factors are applied to our data, the slopes in the target dependence plot straightens out, and the discrepancies in the low A_T region are much smaller. The best fit to all data in this plot gives $\alpha=1.05\pm0.03$, indicating that pions most likely are produced in central collisions.

Measurements were made for pions (E>16 MeV) and protons (E>37 MeV) in coincidence with projectile fragments (F) in the front wall. No significant difference is observed between the energy spectra of inclusive pions and pions emitted in coincidence with a projectile fragment.

The inclusive charge (Z_F) distributions in the front wall are compared to π^+*F (and to p*F, which is very similar to π^+*F). The yields of Z_F from coincidence measurements clearly deviates from the inclusive measurements. The number of events where more than one projectile fragment is emitted simultaneously is estimated to ~6%. Pion (and proton) producing events show a strong suppression of heavy projectile fragments. From this we conclude that pions are produced in collisions with a high degree of projectile breakup, i.e. what normally would be central collisions.

The Z_F yield from π^+*F and p*F has been investigated for the individual elements in the front wall. An enhancement in the yield is found for elements in plane with the range telescope, but on the opposite side of the beam. This enhancement could be expected from pure momentum conservation.

A C K N O W L E D G E M E N T S

These years of graduation have been most stimulating, and I have acquired knowledge both in heavy ion physics and computer programming. Credit should, however, also be given to all friends and colleagues whom have so willingly given their help when I needed it.

First of all, I want to thank my supervisor Bo Jakobsson for readily sharing his time. Also, I highly appreciate his enthusiasm, patience and encouragement.

All my friends at the department are also acknowledged. Especially Lars Carlén and Mats Westenius for computer assistance, Sten Garpman for his help with computer simulations and mfp estimators, Anders Oskarsson for helping me in the pion analysis and Hans Ryde for his encouragement. To the rest of you, thank you all for taking interest and giving assistance.

Last, but not the least, I want to thank my husband Alvar Norén for his encouragement and belief in me, and also for sharing the daily homework without complaint. I also want to thank my now six-year-old son Conny for sharing his mummy with nuclear physics.

Thanks very much all of you, it has really been a great time.

REFERENCES

1. A. Milone, Il Nuovo Cim. Suppl. Al 12(1954)353.
2. S. Tokunaga et al., Il Nuovo Cim. 5(1957)517.
3. H. Yagoda, Il Nuovo Cim. 6(1957)559.
4. E.M. Friedlander and M. Spirchez, Nucl. Sci. Abstr. 15(1961)3457.
5. B. Judek, Can. J. Phys. 46(1968)343.
6. T.F. Cleghorn et al., Can. J. Phys. Suppl. 46(1968)572.
7. B. Judek, Can. J. Phys. 50(1972)2082.
8. P.S. Freier and C.J. Waddington, Astrophys. Space Sci. 38(1975)419.
9. E.M. Friedlander et al., Phys. Rev. Lett. 45(1980)1084.
10. Proc. of 7th High Energy Heavy Ion Study, GSI Darmstadt, Oct. 8-12, 1984, GSI 85-10, March 1985, ISSN 0171-4546(1985).
11. W. Heinrich and H. Drechsel, GSI report 85-10, March 1985, ISSN 0171-4546(1985)539.
12. B.F. Bayman and Y.C. Tang, Phys. Report 147(1987)157.
13. R. Andersson et al., Univ. of Lund, Cosmic Ray Phys. Rep. (1973).
14. S. Beri et al., Z. Phys. A327(1987)431.
15. E.S. Psenin and V.G. Voinov, Phys. Lett. 128B(1983)133.
16. S. Garpman et al., Phys. Rev. Lett. 53(1984)2195.
17. H.B. Barber et al., Phys. Rev. Lett. 48(1982)856.
18. G. Baroni et al., Nucl. Phys. A434(1985)729.
19. R. Silberberg and C.H. Tsao, Proc. 15th Int. Cosmic Ray Conf. Plovdiv (1977) vol. 2, p.89.
20. L. Lyons and G. Gibaut, Phys. Lett. 153B(1985)37.
21. C.M.G. Lattes et al., Nature 159(1947)694.
22. B. Jakobsson, Physica Scripta T5(1983)207.
23. C. Guet and M. Prakash, Nucl. Phys. A428(1984)119c.
24. R. Shyam and J. Knoll, Nucl. Phys. A428(1984)606, A448(1985)322.
25. J. Aichelin and G.F. Bertsch, Phys. Lett. 138B(1984)350.
26. D. Vasak et al., Physica Scripta 22(1980)25, Phys. Lett. 93B(1980)243, Nucl. Phys. A428(1984)291c.
27. W. Benenson et al., Phys. Rev. Lett. 43(1979)683. Errata Phys. Rev. Lett. 44(1980)54.
28. P. Kristiansson, Thesis, Cosmic and Subatomic Physics Report, LUIP 8511.

29. G. Sanouillet et al., CEN, Saclay Internal Report
CEA-N-2483(1986).
30. S. Nagamiya et al., Phys. Rev. C24(1981)971.
31. A. Bonasera and G.F. Bertsch, Phys. Lett. B195(1987)521.
32. L. Westerberg, Nucl. Phys. A447(1985)395c.